Eur. Phys. J. B **18**, 95–101 (2000)

THE EUROPEAN PHYSICAL JOURNAL B

EDP Sciences

Local multifractal thermodynamics of 3D turbulence

A. Bershadskii[1,2,a], T. Nakano[1], D. Fukayama[1], and T. Gotoh[3]

[1] Department of Physics, Chuo University, Tokyo 112 – 8551, Japan
[2] Machanaim Center, PO Box 31155, Jerusalem 91000, Israel
[3] Department of Systems Engineering, Nagoya Institute of Technology, Nagoya 466 – 8555, Japan

Received 21 July 2000

Abstract. Using results of a direct numerical simulation (DNS) of 3D turbulence we show that the observed generalized scaling (*i.e.* scaling moments *versus* moments of different orders) is consistent with a lognormal-like distribution of turbulent energy dissipation fluctuations with moderate amplitudes for *all* space scales available in this DNS (beginning from the molecular viscosity scale up to largest ones). *Local* multifractal thermodynamics has been developed to interpret the data obtained using the generalized scaling, and a new interval of space scales with inverse cascade of generalized energy has been found between dissipative and inertial intervals of scales for sufficiently large values of the Reynolds number.

PACS. 05.45.-a Nonlinear dynamics and nonlinear dynamical systems – 47.27.Ak Fundamentals – 47.27.Gs Isotropic turbulence; homogeneous turbulence

1 Introduction

Generalized scaling, *i.e.* scaling of moments *versus* moments of different orders is now widely used for description of the intermittency phenomenon in turbulence [1–7], in multiparticle production at high energies [8,9], and in surface roughening processes [10]. It is shown in numerous experiments and numerical simulations that the range of applicability of the generalized scaling is substantially larger than that of ordinary scaling, and the generalized scaling can exist even in situations where the ordinary scaling cannot be observed at all. The thermodynamic interpretation of the multifractality used for ordinary scaling (see, for instance, [11]) can be expanded in application to the generalized scaling as well.

In the present paper we use the generalized scaling to analyze data of a direct numerical simulation (DNS) of 3D turbulence and we show that these data are consistent with lognormal-like distribution of turbulent energy dissipation fluctuations with moderate amplitudes for all space scales observed in the DNS (beginning from dissipative scales up to the largest ones). The lognormal distribution for turbulent energy dissipation was suggested for the first time by Obukhov and Kolmogorov and then widely used (see for review [12–14] and references therein), but due to the difficulties to interpret available data of experiments and numerical simulations many other types of distributions were also considered as possible for different values of the fluctuations amplitude and scales (*e.g.* stretched exponential [15], and power-law [16]). Therefore, the finding that turbulent energy dissipation fluctuations with moderate amplitudes possesses lognormal properties for *all* observable space scales (larger than molecular viscous dissipation scale) can give a new insight into this longstanding problem.

Expansion of the multifractal thermodynamics on the region of space scales where ordinary scaling does not exist allows, for the first time, to calculate multifractal entropy *depending* on space scale for the data obtained in a DNS of 3D turbulence. Studying this space scale dependence of multifractal entropy we have found a new interval of scales located between dissipative and inertial intervals, with unusual inverse cascade of the generalized energy for 3D turbulence. This 'inverse' interval appears only for sufficiently large values of Reynolds number ($R_\lambda \geq 459$ according to the present DNS) and for large order of moments of fluctuations of the velocity increment. The critical multifractal temperature, for which the 'inverse' interval appears for the first time, scales (decreases) with the Reynolds number.

The present paper is organized as follows. In Section 2 the generalized scaling for the locally averaged energy dissipation rate is introduced for the lognormal distribution. Then the scaling exponents of the moments of the longitudinal velocity increments are derived on the basis of the locally extended self-similarity method. Section 3 is devoted to the direct numerical simulation. The scaling exponents of the longitudinal structure function are calculated. In Section 4 we compare the scaling exponents calculated for the DNS with the expression resulted from the lognormal distribution. The agreement is quite satisfactory. The comparison enables us to estimate a local

[a] e-mail: bersh@hotmail.com

value of the intermittency factor μ. Interesting things derived from the scale dependence of μ are also presented. In Section 5 local multifractal thermodynamics is developed. It is found that the inverse cascade of the generalized energy can occur for large Reynolds numbers. In Section 6 we summarize what we found in the present work.

2 Generalized scaling in turbulence

For the absolute value of longitudinal velocity increments: $u_r = |v(x+r) - v(x)|$ (over separation r) the generalized scaling means

$$\langle (u_r)^q \rangle \sim \langle (u_r)^p \rangle^{\rho(q,p)} \tag{1}$$

where the scaling exponent $\rho(q,p)$ is some function on q and p. In spite of the intensive studies and great interest the nature of the generalized scaling in turbulent flows is still unclear. It can be shown (see below) that the lognormal distribution itself leads to generalized scaling of the lognormally distributed quantity. Following Kolmogorov and Obukhov [12–14] we consider the lognormal distribution as a possibility for the local average fluctuations of the turbulent energy dissipation field $\varepsilon(\mathbf{x})$

$$\varepsilon_r = \frac{\int_{V_r} \varepsilon(\mathbf{x}) \mathrm{d}V}{V_r} \tag{2}$$

where V_r is an arbitrary space volume with scale r.

If ε_r is lognormally distributed, *i.e.*

$$P(\varepsilon_r) = \frac{\varepsilon_r^{-1}}{(2\pi\sigma^2)^{1/2}} \exp\left[-\frac{(\ln(\varepsilon_r) - a)^2}{2\sigma^2} \right] \tag{3}$$

then we obtain for moments of ε_r

$$\langle \varepsilon_r^q \rangle = \mathrm{e}^{qa + \frac{\sigma^2}{2} q^2} \tag{4}$$

or

$$\frac{\langle \varepsilon_r^q \rangle}{\langle \varepsilon_r \rangle^q} = \mathrm{e}^{\frac{\sigma^2}{2} q(q-1)} \tag{5}$$

that results in some type of generalized scaling of turbulent energy dissipation

$$\frac{\langle \varepsilon_r^q \rangle}{\langle \varepsilon_r \rangle^q} = \left(\frac{\langle \varepsilon_r^p \rangle}{\langle \varepsilon_r \rangle^p} \right)^{\frac{q(q-1)}{p(p-1)}}. \tag{6}$$

Since this generalized scaling describes a more general class of random variables than the lognormal one, we call this class as lognormal-like.

What is the equivalent relation for the velocity increment? According to the refined self-similarity method [12] $u_r \sim (r\varepsilon_r)^{1/3}$ in the inertial region, while $u_r \sim r\varepsilon_r^{1/2}$ in the dissipative region. In order to consider both regions at the same time we assume a general relation

$$u_r = c(r) \varepsilon_r^{1/\beta(r)} \tag{7}$$

in a mean sense (see (6, 8)). Here $\beta(r)$ is a function of r and coefficient $c(r)$ does not necessarily scale with r. Substituting (7) into (6) yields

$$\frac{\langle u_r^q \rangle}{\langle u_r^\beta \rangle^{q/\beta}} \sim \left(\frac{\langle u_r^p \rangle}{\langle u_r^\beta \rangle^{p/\beta}} \right)^{\frac{q(q-\beta)}{p(p-\beta)}}. \tag{8}$$

This relation can be considered as a functional equation and a solution to this equation is

$$\langle u_r^p \rangle \sim \langle u_r^{\beta(r)} \rangle^{p/\beta(r) + b(r)p(p-\beta(r))}, \tag{9}$$

where $b(r)$ is an arbitrary function of r. Relation (9) is a generalization of ordinary extended self-similarity (ESS) [1,2]. The difference between ordinary ESS and relation (9) is that parameters used in (9) can depend on r. Therefore we will call this type of ESS an extended *local* self-similarity (ELSS).

To be consistent with the present data processing we express the pth order structure function in terms of 3rd order structure function as

$$\langle u_r^p \rangle \sim \langle u_r^3 \rangle^{\zeta_p(r)} \tag{10}$$

Making use of (9), we are led to

$$\zeta_p(r) = \frac{p}{3} - \frac{\mu(r)}{18} p(p-3), \tag{11}$$

where

$$\mu(r) = -\frac{6b(r)\beta(r)}{1 + \beta(r)(3 - \beta(r))b(r)}. \tag{12}$$

In the frame of ELSS the exponent ζ_p depends also on r, and below we compare (10) and (11) with data of a DNS for different values of r. It should be noted that the ELSS expression (11) holds for any value of $\beta(r)$, so that the expression can be compared with the data for the inertial separation as well as for the dissipative one.

3 Direct numerical simulation of 3D turbulence and data representation

The simulations are done using Navier-Stokes equation on mesh points up to 1024^3, Reynolds numbers ranging from 50 to 459 [17]. Before going into the details of the present simulation we recall a history of the DNS. In 1981 Siggia [18] started with 64^3 points, and Kerr [19] followed with 128^3 in 1985. In 1991 Vincent and Meneguzzi [20] made simulation on 240^3 with $R_\lambda = 150$, while the simulation on 512^3 points was done in 1993 by Jimenez *et al.* [21] with $R_\lambda = 170$ and by Chen *et al.* [22] with $R_\lambda = 200$. Since then the DNS with larger number of mesh points has not, to our knowledge, been reported in a public Journal. Hence we reached the largest Reynolds number on 1024^3 mesh points here.

Turbulence is continuously excited by the random force which is statistically homogeneous, isotropic and Gaussian white, and whose the spectrum form is constant

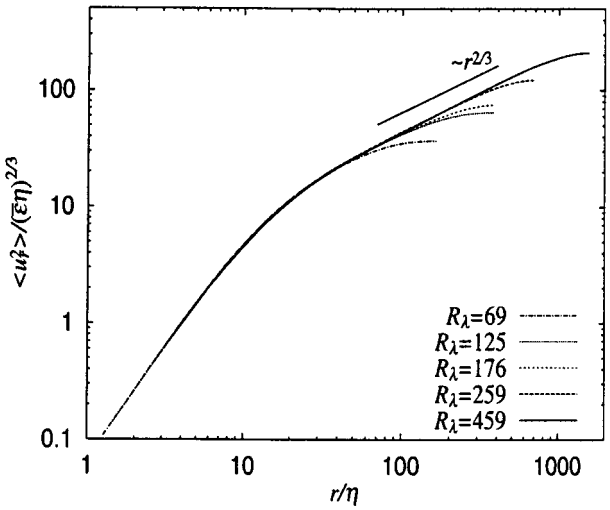

Fig. 1. A plot of $\langle u_r^2 \rangle$ divided by $(\overline{\varepsilon}\eta)^{2/3}$ *vs.* r/η for various values of Reynolds number. An inserted solid line is proportional to $r^{2/3}$. Notice that all data points collapse on a single curve in the dissipative region.

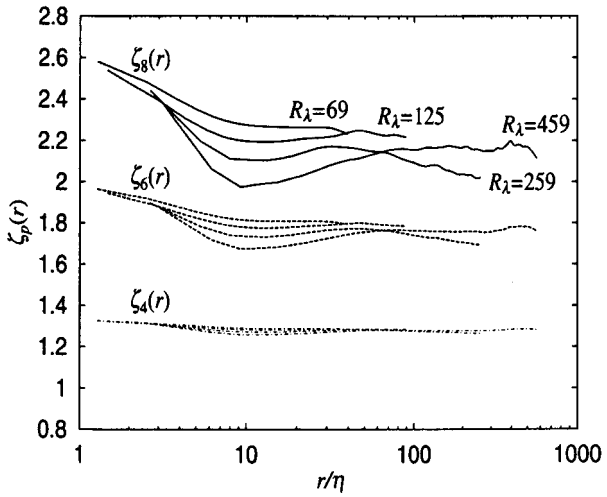

Fig. 2. The ELSS exponents $\zeta_4(r), \zeta_6(r)$ and $\zeta_8(r)$ against r/η for various values of Reynolds number. The data with scales larger than integral scales are deleted from the figure.

in the band spectrum limited to the band $1 < k < 3$. The code uses the pseudo spectral method and the 4th order Runge-Kutta-Gill one. The statistical averages were taken as the time average over tens of turnover times for lower Reynolds numbers and over a few turnover times for the higher Reynolds numbers (the turnover time is a period of time during which the largest eddy turns around once). The data of the highest Reynolds number $R_\lambda = 459$ were obtained as rather short time average (about 1.4 eddy turnover time). The condition for the resolution of DNS $k_{\max}\eta > 1$, where $k_{\max}$ is the largest wavenumber allowed in simulation, is satisfied for most runs, but that of $R_\lambda = 459$ is slightly less than unity. Computations with $R_\lambda \leq 259$ have been done using a vector parallel machine with 16 processors, Fujitsu VPP700E at RIKEN, and those for higher R_λ, using Fujitsu VPP5000/56 with 32 processors at Nagoya University Computation Center.

Now turn to the data analysis. Figure 1 is a plot of $\langle u_r^2 \rangle / (\overline{\varepsilon}\eta)^{2/3}$against r/η for various values of Reynolds number, where $\overline{\varepsilon}$ is the average dissipation rate, and $\eta = (\nu^3/\overline{\varepsilon})^{1/4}$ with molecular viscosity ν. Here a straight solid line proportional to $r^{2/3}$ is inserted. It is remarkable that all data points collapse on a single line in the dissipative region, which indicates that all simulations are carried out with good resolution at small scales. Although the slope of $\langle u_r^2 \rangle$ could be estimated for large Reynolds numbers as seen from Figure 1, the scaling exponents of higher order structure functions as well as low order ones for small Reynolds numbers can be reliably evaluated only on the basis of the ESS method, *i.e.* by plotting $\langle u_r^p \rangle$ against $\langle u_r^3 \rangle$ [1,2].

In order to know the r-dependence of $\zeta_p(r)$ for various Reynolds numbers, we prepare Figure 2, in which $\zeta_p(r)$ with $p = 4, 6, 8$ are depicted for $R_\lambda = 69, 125, 259$ and 459. (The eighth order structure function is confirmed to converge statistically.) Note that the data for scales larger than integral scales, *i.e.* the averaged scales weighted over the energy spectrum [12], because a universal property of turbulence is not reflected in those data. It is remarkable that there is a dip at about $r/\eta \sim 10$, and that it grows in depth with Reynolds number. The exception is the case $R_\lambda = 69$, where a dip does not appear. As the scale increases beyond the dip, $\zeta_4(r)$ and $\zeta_6(r)$ tend to approach constant values, although the corresponding data for $R_\lambda = 259$ behave in a slightly different way from other cases. For $p = 8$ the situation is the same as for $p = 6$, but the fluctuations are larger. It is of interest to notice that for the largest Reynolds number 459 the flat region is observed in the interval $100 < r/\eta < 300$, which may be identified with the inertial region [12]. For smaller Reynolds numbers it is difficult to find the flat region. For $R_\lambda = 69$ we see the flat region in the interval $10 < r/\eta < 30$, and the corresponding slopes for $p \geq 4$ are larger than those for $R_\lambda = 459$. However, the flat region at smaller scales for $R_\lambda = 69$ is different from one at larger scales for $R_\lambda = 459$.

Before concluding this section we depict the probability distribution density of the dissipation field ε for $R_\lambda = 459$ in Figure 3, where the abscissa is $x \equiv (\ln \varepsilon - \langle \ln \varepsilon \rangle)/\sigma$ with σ a standard deviation of $\ln \varepsilon - \langle \ln \varepsilon \rangle$, and the ordinate is the probability density function (PDF) of x. An inserted solid line stands for the lognormal distribution. It is clearly seen that the distribution of the dissipation field is lognormal in the range of small amplitudes.

4 Lognormally generated ELSS and the 3D data

In order to analyze a nature of the r-dependence of the local slope $\zeta_p(r)$, we will rely on the lognormal expression (11). To compare ELSS relations (10, 11) with the data, let us rewrite (11) in the following form:

$$\frac{\zeta_p}{p} = \left(\frac{1}{3} + \frac{\mu(r)}{6}\right) - \frac{\mu(r)}{18}p. \qquad (13)$$

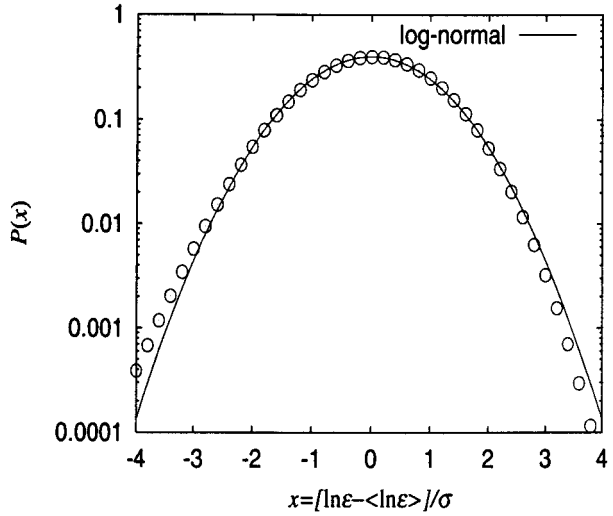

Fig. 3. The probability distribution density of the dissipation field ε for $R_\lambda = 459$, where the abscissa is $x \equiv (\ln\varepsilon - \langle\ln\varepsilon\rangle)/\sigma$ with σ a standard deviation of $\ln\varepsilon - \langle\ln\varepsilon\rangle$, and the ordinate is the PDF of x. An inserted solid line represents for the lognormal distribution.

The comparison of the data with the above representation is limited to $p \leq 6$, but the intermittency coefficient $\mu(r)$ estimated from $p \leq 6$ plays a decisive role to represent even the whole intermittency effect.

Figure 4a shows a curve $\zeta_p(r)/p$ *vs.* p for several values of r/η with $R_\lambda = 69$. Straight lines in this figure are the best fit lines for $1 \leq p \leq 6$. The data points for $p = 7$, which are not included for the comparison, are slightly deviated from the lognormal lines as expected. Intermittency index, $\mu(r)$, can be calculated from this figure using the slope of the fitting straight lines or the intersection point of the fitting straight lines with vertical axis (*cf.* (13)). The calculated values of $\mu(r)$ are shown in the inset of Figure 4a (μ_1 corresponds to calculations using the 'slope' method, whereas μ_2 are given by the 'intersection' method). In the plot of $\mu(r)$ Taylor microscale λ [12] and an integral scale L are marked for convenience. (We have confirmed the well-known prediction [23] $\lambda/\eta = 15^{1/4} R_\lambda^{1/2}$ and $L/\eta \sim R_\lambda^{3/2}$.) For Reynolds numbers 259 and 459 we have obtained similar pictures (Figs. 4b and c). Other Reynolds numbers give the same result.

As seen from Figures 4a to c, $\mu(r)$ substantially depends on r with a typical "two-maxima" shape. Even for $R_\lambda = 69$ in Figure 4a there is a small peak around $r/\eta \sim 10$. Local maximum of the $\mu(r)$ at smaller scales exhibits a few interesting properties. (I) For $R_\lambda = 50$ the maximum is not observed, and the first appearance of the maximum occurs at R_λ between 50 and 69. (II) A position of this maximum (normalized by η) is independent of Reynolds number (see Fig. 5), and takes value $\ell_1 \approx 14\eta$, which is actually the beginning of the dissipative region. (III) Value of $\mu(\ell_1)$ scales with R_λ as $\mu(\ell_1) \sim R_\lambda^{0.26}$ as seen from the inset of Figure 5. (IV) The scale λ is located on the right descending hill.

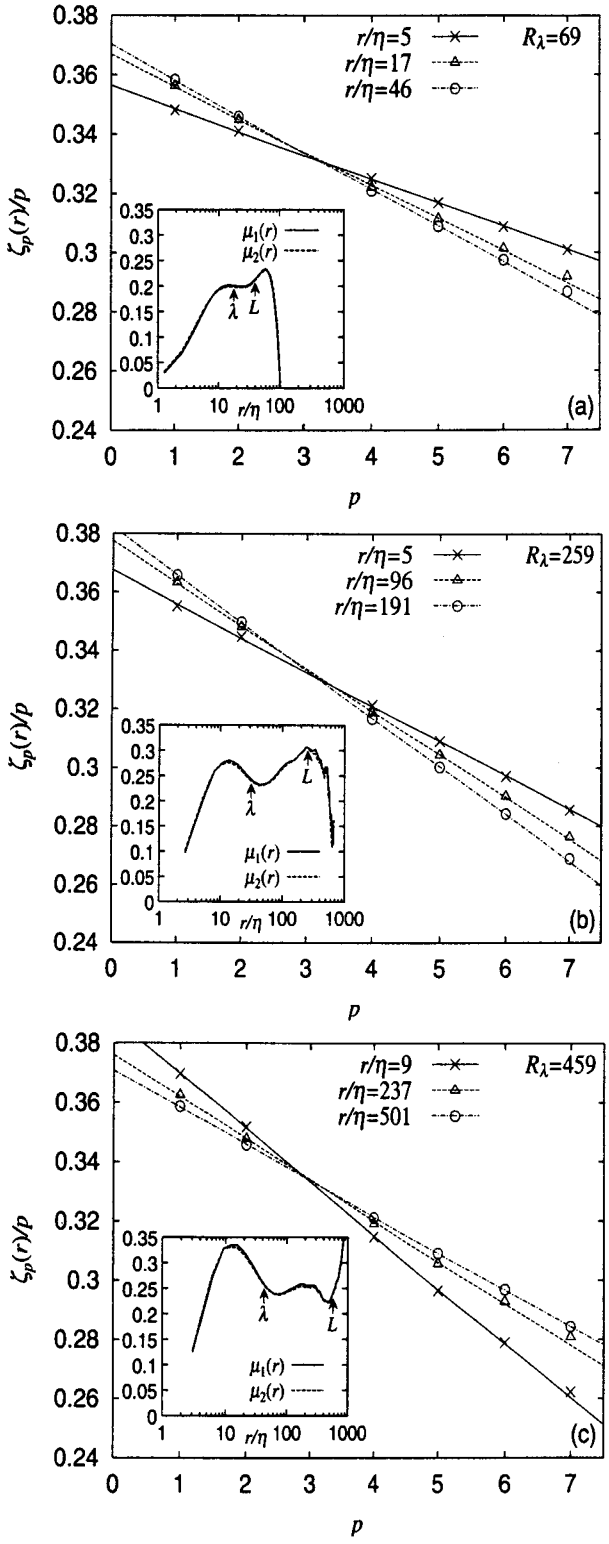

Fig. 4. The ELSS exponents $\zeta_p(r)/p$ against p obtained in the DNS for different values of r and for different Reynolds numbers; (a) $R_\lambda = 69$, (b) $R_\lambda = 259$ and (c) $R_\lambda = 459$. Straight lines, which are the best fit line for $1 \leq p \leq 6$, indicate agreement of the data with the representation (13). The insert shows the local intermittency exponent $\mu(r)$ calculated using the data. $\mu_1(r)$ corresponds to calculations using the 'slope' method (described in the text), and $\mu_2(r)$ does to those using the 'intersection' method. Calculated Taylor length λ and the integral length L are marked for convenience.

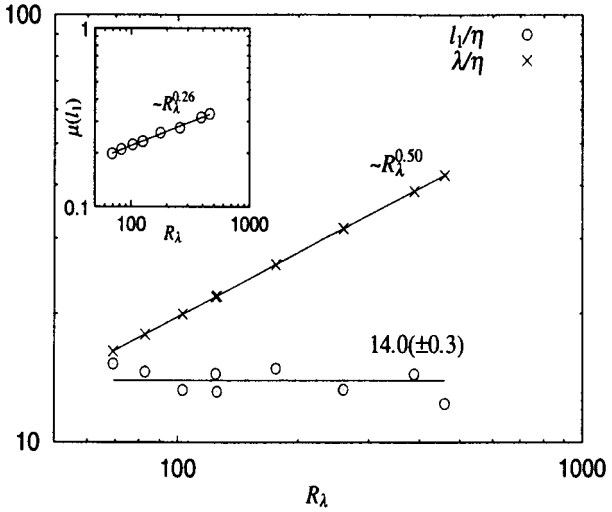

Fig. 5. Different characteristics of the turbulent motion against Reynolds number R_λ. Crosses correspond to λ normalized by η against R_λ. Open circles correspond to position ℓ_1 of the small-scale maximum of the intermittency exponent $\mu(r)$ normalized by η. Insert shows $\mu(\ell_1)$ against R_λ.

The flat region where $\mu(r)$ is constant appears in between $r/\eta \sim 100$ and $r/\eta \sim 300$ for the highest Reynolds number $R_\lambda = 459$ (see Fig. 4c). In such an interval $\mu(r) \approx 0.25$. This value is consistent with those known in literature for observations corresponding to very large Reynolds number [24,25].

It should be noted that strong tube-like vortices are believed to be sparsely distributed in space in fully developed turbulence [21,26,27]. Those vortices are frequently assumed as Burgers' vortex with mean radius 10η [27]. The energy dissipation takes place strongly around those vortices. Therefore extreme intermittency of the energy dissipation at this scale is consistent with the observation of the maximum of $\mu(r)$ at scale $r = 14\eta$. On the other hand, the usual scaling region, where $\zeta_p(r)$ as well as $\mu(r)$ are independent of scale in a certain interval of scale, can be seen only for largest Reynolds number, $R_\lambda = 459$ in the present work. Such a scaling region is located for $r > \lambda$; in our simulation the scaling region starts from approximately 2.5λ.

5 Local multifractal thermodynamics

Let us imagine a grid with a local (cell-) scale r and a global scale L, and label vertices of this grid by symbol i. Let us make a partial average of absolute value of increment of projection of velocity $\mathbf{v}$ along the vector $\mathbf{r}$ (longitudinal increment): $u_r = |v(\mathbf{x_i} + \mathbf{r}) - v(\mathbf{x_i})|$ over all possible directions of the vector $\mathbf{r}$. Let denote this partially averaged increment as $\overline{u_r}$. It is clear that for isotropic turbulence $\overline{u_r}$ will be depending only on $r = |\mathbf{r}|$. Let us define a measure:

$$p_i = \frac{\overline{u_r}^3}{\sum_i^N \overline{u_r}^3} \tag{15}$$

(where $N = (L/r)^3$), and a partition function

$$Z_n = \sum_i^N p_i^n. \tag{16}$$

Let us consider scaling-like behavior of the partition function

$$Z_n \sim \left(\frac{r}{L}\right)^{\tau_n(r)} \tag{17}$$

where exponent $\tau(r)$ depends ('weakly') on r. Now we can calculate corresponding scaling-like behavior of full averaged velocity increment

$$\langle u_r^{3n} \rangle \sim \left(\frac{r}{L}\right)^{\zeta^\star_{3n}(r)} \tag{18}$$

using average over all vertexes of the space grid

$$\langle u_r^{3n} \rangle = \frac{\sum_i^N \overline{u_r}^{3n}}{N} \sim \frac{1}{N} Z_n \left(\sum_i^N \overline{u_r}^3\right)^n$$

we can also write

$$\langle u_r^{3n} \rangle \sim N^{(n-1)} \left(\frac{r}{L}\right)^{\tau_n} \langle u_r^3 \rangle^n. \tag{19}$$

Then, equating (18, 19) we obtain

$$\zeta^\star_{3n} = -3(n-1) + \tau_n + \zeta^\star_3 n \tag{20}$$

If we use the obvious relation $\zeta^\star_{3n} = \zeta^\star_3 \zeta_{3n}$ to substitute lognormal representation of ζ_{3n} (11) into (20) we obtain

$$\tau_n = 3(n-1) - \frac{\zeta^\star_3 \mu}{2} n(n-1) \tag{21}$$

This is lognormal representation of the multifractal exponent τ_n.

Now let us introduce local multifractal thermodynamics. Let the measure p_i scale as

$$p_i \sim \left(\frac{r}{L}\right)^{\alpha_i(r)}. \tag{22}$$

Then for $r/L \to 0$ we can estimate partition function as

$$Z_n \sim \int \left(\frac{r}{L}\right)^{n\alpha} N(\alpha) \mathrm{d}\alpha \tag{23}$$

where $N(\alpha)$ is distribution of the exponents α over the grid vertices and we also suppose that

$$N(\alpha) = \rho(\alpha) \left(\frac{r}{L}\right)^{-f_\alpha} \tag{24}$$

For the monofractal case $N(\alpha) = \left(\frac{r}{L}\right)^{-d}$, but for the multifractal situation f_α is a function of α. It is easy to show (see, for instance, [11]) that for $r/L \to 0$

$$\tau_n = n\alpha - f_\alpha \tag{25}$$

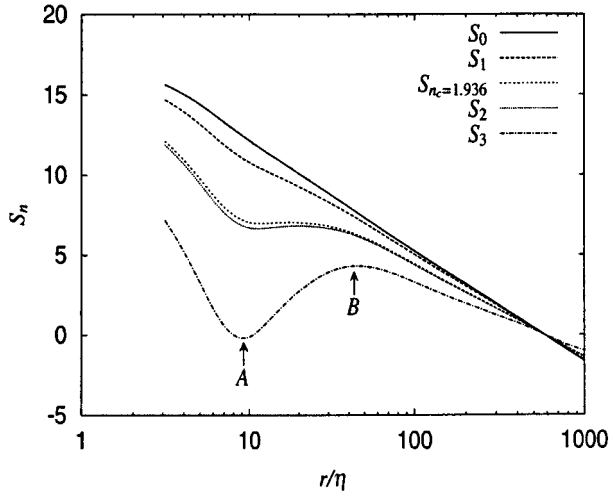

Fig. 6. Multifractal entropy S_n *vs.* r/η for $R_\lambda = 459$ and for different values of the multifractal inverse temperature n_c.

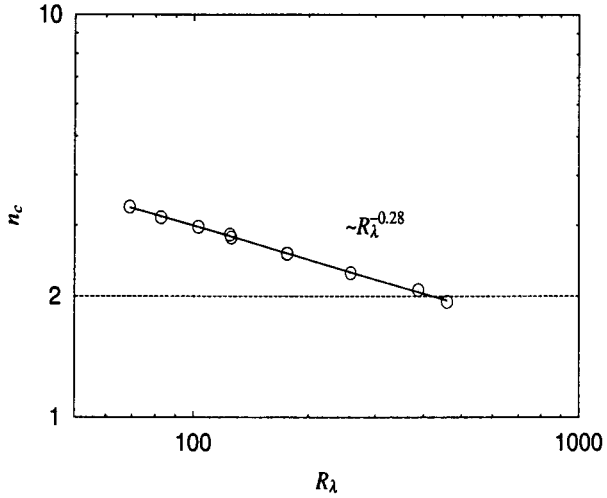

Fig. 7. Scaling of the critical inverse temperature n_c with R_λ. The straight dashed line $n_c = 2$ ($p = 6$) is the line, below which the lognormal assumption is consistent with the DNS data in quite a satisfactory way.

if

$$\frac{\mathrm{d}f}{\mathrm{d}\alpha} = n. \tag{26}$$

Using lognormal representation (21) and relations (25, 26) one can calculate lognormal representation of the multifractal index f as function of n

$$f = 3 - \frac{\zeta_3^\star \mu}{2} n^2. \tag{27}$$

In the ordinary thermodynamics the Maxwell-Boltzmann partition function is

$$Z_\beta = \int \mathrm{e}^{-\beta E} N(E) \mathrm{d}E \tag{28}$$

where E is thermodynamic energy, $N(E)$ distribution of the energy, and β is inverse temperature. To compare the multifractal partition with the thermodynamic one let us rewrite (23) as

$$Z_n \sim \int \mathrm{e}^{-\ln(L/r)\alpha n} N(\alpha) \mathrm{d}\alpha \tag{29}$$

From comparison of (28) with (29) we can associate $\ln(L/r)\alpha$ with thermodynamic energy E and the order parameter n with inverse temperature. Then, by comparing the thermodynamic relation

$$\frac{\mathrm{d}S}{\mathrm{d}E} = \beta \tag{30}$$

with the multifractal relation (26) we can associate $\ln(L/r)f(n)$ with entropy S. Now we can calculate the multifractal entropy corresponding to the lognormal distribution using (27)

$$S_n = \ln(L/r) f(n) = \ln(L/r) \left(3 - \frac{\zeta_3^\star(r)\mu(r)}{2} n^2 \right). \tag{31}$$

Note that S_n is the multifractal entropy defined for $\langle u_r^{3n} \rangle$.

In Figure 6 we show calculated results of the multifractal entropy against r/η performed for different values of multifractal inverse temperature n using (31) and the data obtained in the DNS for $R_\lambda = 459$ (for other values of the Reynolds number the picture is qualitatively the same). We can see that for sufficiently large inverse temperatures n some local minimum and maximum appear in the multifractal entropy as seen in Figure 6.

In the interval of scales located between the local minimum indicated by arrow A and maximum by arrow B the multifractal entropy *increases* with r while outside this interval the multifractal entropy decreases with r. Increasing the entropy with decreasing value of r means that structures with larger scales are thermodynamically unstable and break down, generating smaller ones, while decreasing the entropy with decreasing value of r means a reverse process. The former situation is called as usual cascade process from large to small scales, while the latter situation can be interpreted as an inverse cascade of the generalized energy denoted by $\langle u_r^{3n} \rangle$. As we can see from Figure 6 an interval with inverse cascade (or inverse interval) appears only for sufficiently large inverse temperature n (in particular, for ordinary energy $\langle u_r^2 \rangle$ we have no interval with inverse cascade at values of Reynolds number realized in this DNS). Let us denote the 'critical' value of the inverse temperature (when the inverse interval appears for the first time) as n_c; the inverse cascade occurs *only* for $n \geq n_c$. Figure 7 shows the dependence of the inverse critical temperature on the Reynolds number. We can see that n_c scales (decreases) with R_λ. Note that the value of the inverse multifractal temperature n_c is related to the corresponding value p_c of the order of velocity increment momentum as $p_c = 3n_c$ (see (11, 20)).

We have good agreement between the lognormal representation (13) and the DNS data up to $p = 6 \sim 7$ and this value seems to be independent of Reynolds number. On the other hand, decreasing with R_λ (by scaling way) n_c

reaches the value approximately equal 2 (that corresponds to $p = 6$) for $R_\lambda \simeq 459$. It means that for $R_\lambda < 459$ we cannot interpret the inverse intervals as really observed, and only beginning from $R_\lambda \sim 459$ we can really observed existence of such an interval. However, the scaling dependence observed in Figure 7 (which is already reaching the necessary value of $n < 2$, that corresponds to $p < 6$) seems to be available for an extrapolation. Therefore, we can predict appearance of the inverse interval of scales in 3D turbulence for $R_\lambda \geq 459$.

6 Summary

1. The consistency of the DNS data with ELSS related to the lognormal distribution of the turbulent energy dissipation fluctuations with moderate amplitudes for all space scales beginning from the molecular viscous scale η and up to largest ones, and in a wide range of Reynolds numbers: $69 < R_\lambda < 459$, can be considered as a serious indication that turbulent energy dissipation fluctuations have probability density function with lognormal-like behavior in its central part at all scales larger than the molecular viscosity scale η and for all moderate 'turbulent' values of Reynolds numbers. It gives a support for substantial extension of the original Kolmogorov-Obukhov hypothesis of the lognormal PDF, which was suggested for the inertial interval only.
2. The scale $r/\eta \simeq 14$ can be considered as an 'universal' (independent of Reynolds number) scale separating effectively intermittent and dissipative ranges of scales.
3. An interval of scales with inverse cascade properties is found to appear between inertial and dissipative intervals of 3D turbulence for sufficiently large values of Reynolds number (estimated as $R_\lambda \geq 459$).

The work of T.G. presented here was supported by a Grant-in Aid for Scientific Research (C-2) 12640118 from the Japan Society for the Promotion of Science. We are very grateful to RIKEN Computer Center and Nagoya University Computer Center for their support. T. Ochiai at NIT is also acknowledged for his assistance in numerical computation. Comments and suggestions of C.H. Gibson, D. Stauffer and K.R. Sreenivasan were very useful on different stages of the work.

References

1. R. Benzi, S. Ciliberto, R. Tripiccione, C. Baudet, F. Massailoli, S. Succi, Phys. Rev. E **48**, R29 (1993).
2. R. Benzi, S. Ciliberto, C. Baudet, G.R. Chavarria, Physica D **80**, 385 (1995).
3. B. Dhruva, Y. Tsuji, K.R. Sreenivasan, Phys. Rev. E **56**, R4928 (1997).
4. K.R. Sreenivasan, B. Dhruva, Progr. Theor. Phys. Suppl. **130**, 103 (1998).
5. S. Grossmann, D. Lohse, A. Reech, Phys. Rev. E **56**, 5473 (1997).
6. A. Bershadskii, Europhys. Lett. **39**, 587 (1997).
7. D. Fukayama, T. Oyamada, T. Nakano, T. Gotoh, K. Yamamoto, J. Phys. Soc. Jpn **69**, 701 (2000).
8. E.A. De Wolf, I.M. Dremin, W. Kittel, Phys. Rep. **270**, 1 (1996).
9. A. Bershadskii, Phys. Rev. C **59**, 364 (1999).
10. A. Kundagrami *et al.*, Phys. Rev. E **57**, R3703 (1998).
11. H.E. Stanley, P. Meakin, Nature **335**, 405 (1988).
12. A.C. Monin, A.M. Yaglom, *Statistical Fluid Mechanics* (MIT Press, Cambridge, Mass., 1973), Vol. II.
13. C.H. Gibson, Proc. Roy. Soc. London Ser. A **434**, 149 (1991).
14. S. Chen, K.R. Sreenivasan, M. Nelkin, Phys. Rev. Lett. **79**, 1253 (1997).
15. P. Kailasnath, K.R. Sreenivasan, G. Stolovitzsky, Phys. Rev. Lett. **68**, 2766 (1992).
16. M. Yamada, S. Kida, K. Ohkitani, in *Unstable and Turbulent Motion of Fluid*, edited by S. Kida (World Scientific 1993), p. 188.
17. T. Gotoh, D. Fukayama, `nlin/0005012.`
18. E.D. Siggia, J. Fluid Mech. **107**, 375 (1981).
19. R.M. Kerr, J. Fluid Mech. **153**, 31 (1985).
20. A. Vincent, M. Meneguzzi, J. Fluid Mech. **225**, 1 (1991).
21. J. Jimenez, A.A. Wray, P.G. Safman, R.S. Rogallo, J. Fluid Mech. **255**, 65 (1993).
22. S. Chen, G. Doolen, R.H. Kraichnan, Z.S. She, Phys. Fluids A **5**, 458 (1993).
23. H. Tennekes, J.L. Lumley, *First course in turbulence* (MIT Press, Cambridge, 1972).
24. K.R. Sreenivasan, P. Kailasnath, Phys. Fluids A **5**, 512 (1993).
25. A. Praskovsky, S. Oncley, Phys. Fluids A **6**, 2886 (1994).
26. J. Jimenez, A.A. Wray, J. Fluid Mech. **373**, 255 (1998); related references therein.
27. T. Miyauchi, T. Tanahashi, *Proc. of IUTAM Symposium on "Geometry and Statistics of Turbulence", 1999* (Kluwer, to be published).